

# Proceedings of the Institution of Mechanical Engineers, Part C: Journal of Mechanical Engineering Science

<http://pic.sagepub.com/>

---

## Uniaxial tensile fracture of stainless steel–aluminium bi-metals

D-H Zhang, C Guo and X-P Du

*Proceedings of the Institution of Mechanical Engineers, Part C: Journal of Mechanical Engineering Science* 2011 225: 1061

DOI: 10.1177/2041298310393445

The online version of this article can be found at:

<http://pic.sagepub.com/content/225/5/1061>

---

Published by:



<http://www.sagepublications.com>

On behalf of:



[Institution of Mechanical Engineers](http://www.institutionofmechanicalengineers.org)

**Additional services and information for *Proceedings of the Institution of Mechanical Engineers, Part C: Journal of Mechanical Engineering Science* can be found at:**

**Email Alerts:** <http://pic.sagepub.com/cgi/alerts>

**Subscriptions:** <http://pic.sagepub.com/subscriptions>

**Reprints:** <http://www.sagepub.com/journalsReprints.nav>

**Permissions:** <http://www.sagepub.com/journalsPermissions.nav>

**Citations:** <http://pic.sagepub.com/content/225/5/1061.refs.html>

>> [Version of Record](#) - Apr 28, 2011

[What is This?](#)

# Uniaxial tensile fracture of stainless steel–aluminium bi-metals

D-H Zhang<sup>1,2\*</sup>, C Guo<sup>1</sup>, and X-P Du<sup>1</sup>

<sup>1</sup>The School of Mechanical Engineering, Xi'an Jiaotong University, Shaanxi, Xi'an, People's Republic of China

<sup>2</sup>Mechanical and Electrical Engineering Institute, Zhengzhou University of Light Industry, Henan, Zhengzhou, People's Republic of China.

*The manuscript was received on 24 March 2010 and was accepted after revision for publication on 17 December 2010.*

DOI: 10.1177/2041298310393445

**Abstract:** The mechanical behaviour of aluminium 1A30–stainless steel 1Cr18Ni9Ti bi-metals, made by the explosive welding method, is investigated under uniaxial tension conditions. The mechanical parameters of the bi-metal calculated using the mixture rule theory under uniaxial tension conditions are compared with measured parameters. It is found that the mixture rule theory is suitable for the calculation of the mechanical parameters except for ultimate tensile strength. Experimental data show that yield stress and ultimate tensile strength have an exponential relationship with the relative thickness ratio of stainless steel, respectively. A mathematical model is introduced to describe the relationships of yield stress and ultimate tensile strength to the relative thickness ratio of stainless steel. It is also found that elastic modulus, hardening coefficient, and hardening exponent basically have a linear relationship with the absolute thickness ratio of stainless steel, respectively. All the relationships show a monotonically increasing tendency. Fracture behaviour under uniaxial tensile conditions mainly take the form of fracture on the stainless steel side of the bi-metal and detachment in the interface.

**Keywords:** anisotropy, fracture, explosive welding, bi-metal, mixture rule, strain

## 1 INTRODUCTION

Stainless steel–aluminium bi-metals are increasingly used as typical materials for pressure vessels due to their favourable properties, such as corrosion resistance and lower cost. However, since stainless steel and aluminium alloy (both are regarded as single-material metals in this paper) show intensely different structures and mechanical properties, their yield and failure are extremely difficult to occur on the same time during the uniaxial tensile processing of stainless steel–aluminum bi-metals. Hence, compared to a single-material metal, a bi-metal presents

various localized or global deformation and fracture behaviours due to the distinctive properties of its individual components. Similarly, because of the differences in element material properties and the individual components in interface are difficult to identify, the bi-metal may fracture on the lower strength side under an unexpected stress. The fracture behaviours of bi-metals along the lower strength side restrain their applications. A large number of theoretical studies have been made on fracture of the bi-material including elastic–elastic materials [1, 2] and elastic–plastic materials [3–6], with the expectation of finding a bi-material that can overcome the above-mentioned defects. Numerical simulations have been carried out using finite-element analysis [7, 8] to obtain elastic–plastic fracture properties, which include  $J$ - [9] and  $Q$ -resistance [5]. Two analytical models, which are, respectively, based on the upper bound method and the slab method, have been introduced by Hungsiou and Gowyi [10] to describe double-layer clad sheet compression forming. Polymethylmethacrylate/acrylic and aluminium alloy 2024 T531 have been joined

\*Corresponding author: Xi'an Jiaotong University, The School of Mechanical Engineering, Shaanxi, Xi'an 710049, People's Republic of China.

Mechanical and Electrical Engineering Institute, Zhengzhou University of Light Industry, Henan, Zhengzhou, People's Republic of China.

email: zhangdehai0318@163.com

together using epoxy resin [11]. Their study indicates that the bi-material fatigue crack growth is dominantly elastic, with a small plastic zone near the crack tip. Two formulae have been established to correlate the relative thickness of the bi-metal components to the tensile properties of the bi-metal system [12]. The results reveal crack deviation into the under clad soft coarse grained region band due to the strength mismatching the nature of the bi-metal system. Lei and Neale [13] have reviewed the fracture behaviour of a bi-material plate with a through-crack subject to tension. They consider the bi-material plate as a homogeneous material. Plasticity analyses with particular attention to near-tip shielding and amplification have been reported by Sugimura *et al.* [14]. The above studies mainly emphasize the theoretical analysis and static load. Theoretical–experimental studies on material failure mode and mechanism are needed to shed light on the mechanical properties of bi-materials.

In the present work, the authors are interested in uniaxial tensile fracture behaviours of the stainless steel–aluminium bi-metal, which is made of aluminium 1A30 and stainless steel 1Cr18Ni9Ti by the explosive welding method. The mechanical parameters of stainless steel–aluminium under uniaxial tension conditions obtained by the mixture rule method are compared with the experimental data to examine whether the mixture rule method is suitable for the calculation of the bi-metal parameters. Based on the experimental data, two types of relationships are discussed: the relationships of the relative thickness ratio of the stainless steel to yield stress and ultimate tensile strength, and the relationships of the absolute thickness ratio of stainless steel to elastic modulus, hardening coefficient, and hardening exponent. Cross-section scanning is also conducted to analyse the tensile fracture of the bi-metal using scanning electron microscope (SEM) microscopy.

## 2 THE THEORETICAL BASIS

### 2.1 Basic assumptions

To simplify the complication in establishing a bi-metal analytical model, some assumptions are employed throughout the analysis as follows.

1. Interface of the bi-metal is an ideal layer with zero thickness. Such bi-metal shows extremely strong bonding and proportional deformation.
2. The bi-metal presents an anisotropic feature in the thicknesses direction, while each single layer of the bi-metal shows an isotropic feature.
3. The localized and dispersed necking theory is fit for single-layer metal and bi-metal.
4. The strain, strain ratio, and mechanical properties of each layer are assumed to be constant.

### 2.2 The absolute thickness ratio and relative thickness ratio of stainless steel

Since mechanical properties of stainless steel and aluminium are very different, the tensile properties of stainless steel–aluminium bi-materials are determined by the relative ratio of stainless-steel thickness to aluminium thickness according to the mixture rule theory. In this article, stainless steel is used as the substrate material and aluminium as the clad material. The relative ratio of stainless-steel thickness to aluminium thickness  $\wp$  is defined as follows

$$\wp = \frac{t_{\text{stainless}}}{t_{\text{al}}} \quad (1)$$

where  $t_{\text{stainless}}$  and  $t_{\text{al}}$  are the thickness of stainless steel and aluminium, respectively.

The absolute ratios of stainless-steel thickness and aluminium thickness to the total thickness of the bi-metal,  $\mathfrak{R}_{\text{stainless}}$  and  $\mathfrak{R}_{\text{al}}$ , are described as

$$\left. \begin{aligned} \mathfrak{R}_{\text{stainless}} &= \frac{t_{\text{stainless}}}{t} \\ \mathfrak{R}_{\text{al}} &= \frac{t_{\text{al}}}{t} \end{aligned} \right\} \quad (2)$$

where  $t$  denotes the total thickness of the bi-metal.

### 2.3 Analysis of elastic deformation stage

When the bi-metal is under uniaxial tensile force (Fig. 1), according to the force balance conditions, elastic modulus  $E$  of the bi-metal can be obtained as follows

$$E = \mathfrak{R}_{\text{stainless}} E_{\text{stainless}} + \mathfrak{R}_{\text{al}} E_{\text{al}} \quad (3)$$

where  $E_{\text{stainless}}$  and  $E_{\text{al}}$  denote the elastic modulus of stainless steel and aluminium, respectively.

### 2.4 Analysis of plastic deformation stage

The true stress–strain functions, which conform to Holloman's power formulations, are introduced as the follows

$$\left. \begin{aligned} \bar{\sigma}_{\text{stainless}} &= K_{\text{stainless}} \epsilon^{\bar{n}_{\text{stainless}}} \\ \bar{\sigma}_{\text{al}} &= K_{\text{al}} \epsilon^{\bar{n}_{\text{al}}} \\ \bar{\sigma}_{\text{com}} &= K_{\text{com}} \epsilon^{\bar{n}_{\text{com}}} \end{aligned} \right\} \quad (4)$$

where  $\bar{\sigma}_{\text{stainless}}$ ,  $\bar{\sigma}_{\text{al}}$ , and  $\bar{\sigma}_{\text{com}}$  denote the equivalent stress of stainless steel, aluminium, and bi-metal,

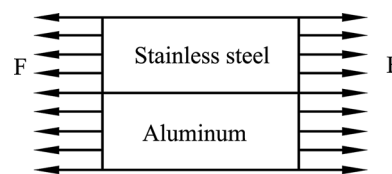


**Fig. 1** Schematic diagram of the bi-metal under uniaxial tensile

respectively.  $K_{\text{stainless}}$ ,  $K_{\text{al}}$ , and  $K_{\text{com}}$  are their hardening coefficients and  $\bar{n}_{\text{stainless}}$ ,  $\bar{n}_{\text{al}}$ , and  $\bar{n}_{\text{com}}$  represent their hardening exponents, respectively.  $\varepsilon$  is the true strain. According to the mixture rule theory, the force balance conditions along the three-dimensional directions can be expressed as follows

$$\left. \begin{aligned} \sigma_{\text{stainless}}^1 \mathfrak{N}_{\text{stainless}} + \sigma_{\text{al}}^1 \mathfrak{N}_{\text{al}} &= \sigma_{\text{com}}^1 \\ \sigma_{\text{stainless}}^2 \mathfrak{N}_{\text{stainless}} + \sigma_{\text{al}}^2 \mathfrak{N}_{\text{al}} &= \sigma_{\text{com}}^2 \\ \sigma_{\text{stainless}}^3 &= \sigma_{\text{al}}^3 = \sigma_{\text{com}}^3 = 0 \end{aligned} \right\} \quad (5)$$

where  $\sigma_{\text{com}}^1$ ,  $\sigma_{\text{com}}^2$ , and  $\sigma_{\text{com}}^3$  are the stress along the directions of the length, width, and thickness of the bi-metal;  $\sigma_{\text{stainless}}^1$ ,  $\sigma_{\text{stainless}}^2$ , and  $\sigma_{\text{stainless}}^3$  are the stress along the directions of the length, width, and thickness of stainless steel; and  $\sigma_{\text{al}}^1$ ,  $\sigma_{\text{al}}^2$ , and  $\sigma_{\text{al}}^3$  are the stress along the directions of the length, width, and thickness of aluminium. In this study, yield strength and ultimate tensile strength of the bi-metal are calculated using equation (5).

After necking, regression line and hardening exponent  $n$  are obtained using the least squares and the linear regression methods. According to the two methods, no less than five true stress–strain points with equal intervals should be chosen from the yield stress to the maximum loading to calculate the hardening exponent. The calculation formula is obtained as follows

$$n = \frac{N \sum_{i=1}^N X_i Y_i - \sum_{i=1}^N X_i \sum_{i=1}^N Y_i}{N \sum_{i=1}^N (X_i)^2 - (\sum_{i=1}^N X_i)^2} \quad (6)$$

where  $N$  is the number of true stress–strain points for regressing calculation, and  $X_i = \log \varepsilon$  and  $Y_i = \log \sigma$ . The intercept  $b$  and hardening coefficient  $K$  are obtained by equation (7)

$$\left\{ \begin{aligned} b &= \frac{\sum_{i=1}^N Y_i - \sum_{i=1}^N X_i}{N} \\ K &= \exp(b) \end{aligned} \right. \quad (7)$$

**2.5 Hill’s localized necking conditions**

On the basis of Hill’s yield criteria, stress and strain increments of each layer of the bi-metal are obtained as follows

$$B^{(i)} = \left. \begin{aligned} \bar{\sigma}^{(i)} &= \sigma_1^{(i)} / B^{(i)} \\ &\sqrt{\frac{4(2 + \gamma^{(i)})}{3(1 + \gamma^{(i)})} \left[ 1 - \frac{2r^{(i)}}{1 + \gamma^{(i)}} \alpha^{(i)} + (\alpha^{(i)})^2 \right]^{-\frac{1}{2}}} \end{aligned} \right\} \quad (8)$$

$$C^{(i)} = \left. \begin{aligned} d\bar{\varepsilon}^{(i)} &= C^{(i)} d\varepsilon_1 \\ &\sqrt{\frac{2(2 + \gamma^{(i)})(1 + \gamma^{(i)})}{3(1 + 2\gamma^{(i)})} \left( \beta^2 + \frac{2\gamma^{(i)}}{1 + r^{(i)}} \beta + 1 \right)} \end{aligned} \right\} \quad (9)$$

where  $\bar{\sigma}^{(i)}$ ,  $\sigma_j^{(i)}$  ( $j = 1, 2, 3$ ),  $d\bar{\varepsilon}^{(i)}$ ,  $d\varepsilon_j^{(i)}$  ( $j = 1, 2, 3$ ),  $\gamma^{(i)}$ , and  $\alpha^{(i)}$  denote the equivalent stress, principal stress, equivalent strain increment, strain increment, plastic strain ratio, and stress ratio of the  $i$ th-layer material, respectively.  $\beta$  is the strain ratio.

The relationships between the plastic strain ratio and stress ratio are as follows

$$\left. \begin{aligned} \beta &= \frac{\alpha^{(i)}(1 + \gamma^{(i)}) - \gamma^{(i)}}{1 + \gamma^{(i)} - \gamma^{(i)}\alpha^{(i)}} \\ \alpha^{(i)} &= \frac{\beta + \gamma^{(i)} + \beta\gamma^{(i)}}{1 + \gamma^{(i)} + \beta\gamma^{(i)}} \end{aligned} \right\} \quad (10)$$

According to Hill’s localized necking theory, a zero-strain line exists in the tensile-compression area of the bi-metal. When the load reaches the maximum, necking in sheet metal begins to occur. Therefore, the mathematical formula of necking is obtained as follows

$$dF_V = \sum_i \mathfrak{N}^i d(A_V^{(i)} \sigma_V^{(i)}) = 0 \quad (11)$$

where  $A_V$  and  $\sigma_V$  denote interfacial area and stress perpendicular to necking, respectively. Since  $dA_V^{(i)} / A_V^{(i)} = -d\varepsilon_V$ , equation (11) can be expressed as

$$\sum_i \mathfrak{N}^{(i)} \left[ \frac{d\sigma_V^{(i)}}{d\varepsilon_V} - \sigma_V^{(i)} \right] = 0 \quad (12)$$

where  $\mathfrak{N}^{(i)}$  denotes the absolute thickness ratio of the  $i$ th layer.

According to equations (8) to (12), Hill’s localized necking conditions for bi-metals is described as

**Table 1** Mechanical parameters of the bi-metal plate

Material	Elastic moduls (GPa)	Yield stress (MPa)	Ultimate tensile strength (MPa)	K (Mpa)	$n$
1A30	59.8	134.37	150.3	86.59	0.35
1cr18Ni9Ti	171.1	569.15	875.22	358.31	0.29

**Table 2** Yield stress and ultimate tensile strength of the bi-metal material

$\rho$	$\mathfrak{N}_{\text{stainless}}$	$\sigma_s$ (Mpa)		$\sigma_b$ (Mpa)	
		Experiment	Mixing rule	Experiment	Mixing rule
0	0	134.37	134.37	150.3	150.3
0.3	0.24	240.96	238.79	294.56	324.3
0.4	0.28	263.64	256.19	314.33	353.3
0.63	0.39	292.47	304.05	387.13	433
1.06	0.52	367.18	360.61	457.77	527.3
1.95	0.66	391.83	421.52	556.24	628.8
2.96	0.75	465.43	460.68	641.12	694
5	0.83	499.51	495.49	728.94	752
$\infty$	1	569.45	569.45	875.22	875.2

follows

$$\sum_i \mathfrak{R}^{(i)} B^{(i)} \frac{1 - \alpha\beta}{1 - \beta} \left[ \frac{C^{(i)}}{1 + \beta} \frac{d\bar{\sigma}^{(i)}}{d\bar{\epsilon}} - \bar{\sigma}^{(i)} \right] = 0 \quad (13)$$

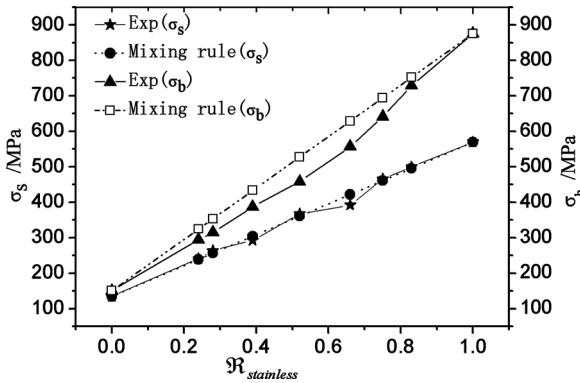


**Fig. 2** Relationship of yield stress and ultimate tensile strength to  $\mathfrak{R}_{\text{stainless}}$   
 Annotation:  $\sigma_s$  and  $\sigma_b$  stand for yield stress and ultimate tensile strength, respectively.

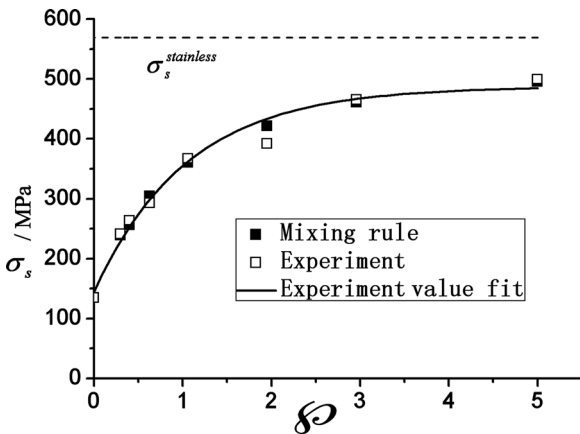


**Fig. 3** Relationship between yield stress and  $\phi$

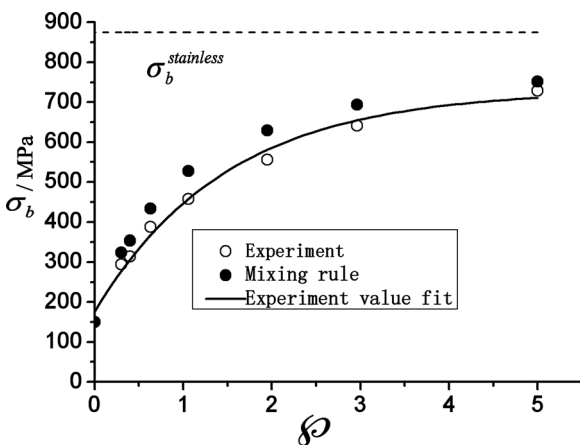


**Fig. 4** Relationship between ultimate tensile strength and  $\phi$

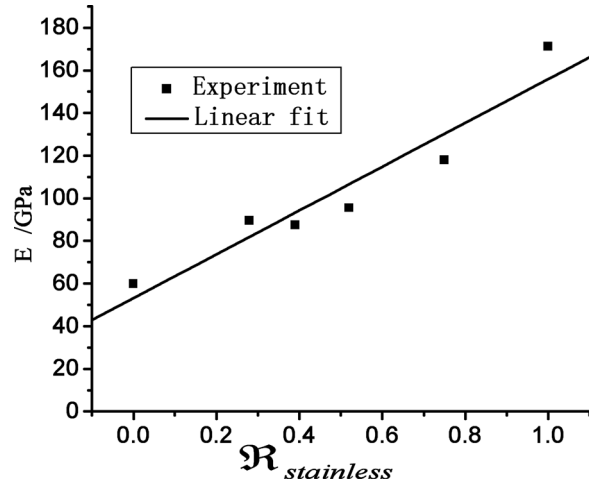


**Fig. 5** Relationship between the elastic modulus and  $\mathfrak{R}_{\text{stainless}}$

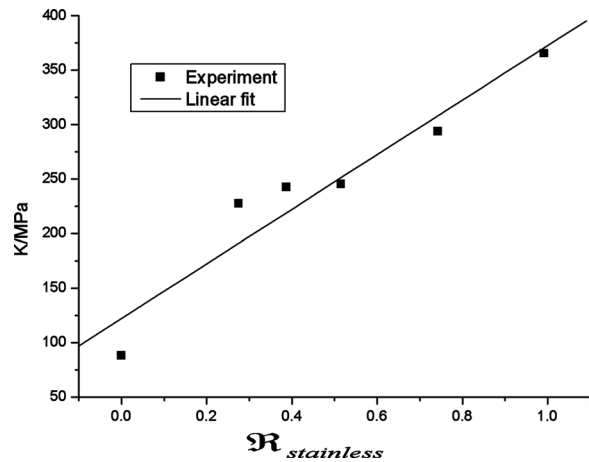


**Fig. 6** Relationship between the hardening coefficient and  $\mathfrak{R}_{\text{stainless}}$

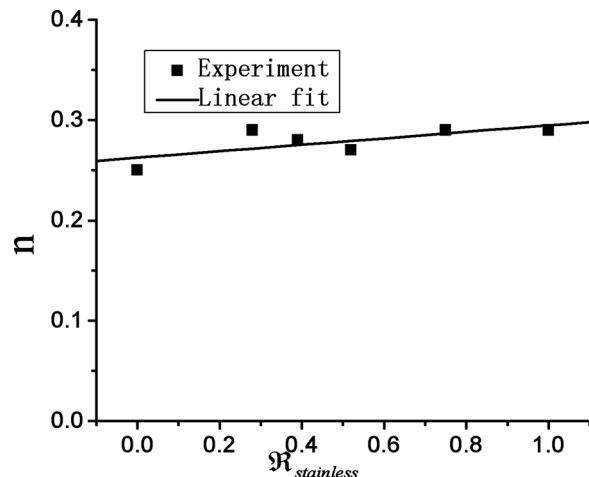


**Fig. 7** Relationship between the hardening exponent and  $\mathfrak{R}_{\text{stainless}}$

### 3 EXPERIMENT

The bi-metal plate used in the study is directly purchased from the Chinese market. The bi-metal is made using aluminium (1A30, China – National Standard Guideline) as substrate (3 mm) and stainless steel (1Cr18Ni9Ti, China – National Standard Guideline) as clad (3 mm) by explosive welding. Uniaxial tensile test is conducted using an Instron-1341 Electron Mul-function Materials Testing Machine. According to No. GB/T 228, the Technical Guidelines for Metals in China, three specimens are, respectively, extracted using the wire cutting method from the substrate, clad, and bi-metal along directions that are 0°, 45°, and 90° to the welding horizontal plane. These specimens are used to determine their mechanical properties under uniaxial tensile conditions. The uniaxial tensile speed is set to be 1 mm/min, and the measured mechanical parameters are given in Table 1.

The fractured specimens are examined using S-3000SEM microscopy (Hitachi Company, Japan) for characterization of the fracture type and crack path.

### 4 RESULTS AND DISCUSSIONS

#### 4.1 The relationships of yield stress and ultimate tensile strength of the bi-metal and relative thickness ratio $\varphi$ and absolute thickness ratio of stainless steel $\mathfrak{R}_{\text{stainless}}$

The yield stress and ultimate tensile strength of the bi-metal are obtained using equation (5); the relative and absolute thickness ratios of stainless steel,  $\varphi$

and  $\mathfrak{R}_{\text{stainless}}$ , are calculated using equations (1) and (2), respectively. The comparison results of the experimental values and the calculated values are shown in Table 2.

The relationships of yield stress  $\sigma_s$  and ultimate tensile strength  $\sigma_b$  to  $\mathfrak{R}_{\text{stainless}}$  are shown in Fig. 2. It can be seen that the yield stress of the bi-metal calculated using the mixture rule theory is basically similar to the experimental value. However, the calculated ultimate tensile strength is much larger than the experimental value. The results show that the mixing rule theory can only be used to calculate the yield stress of the 1A30–1Cr18Ni9Ti bi-metal; however, it is inappropriate for the calculation of the ultimate tensile strength.

As shown in Fig. 3, when  $\varphi$  approaches infinity, the fitting curve of the experimental bi-metal data infinitely approaches the line which represents the calculated yield stress of stainless steel. Figure 4 shows that when  $\varphi$  approaches infinity, the fitting curve of the experimental bi-metal data infinitely approaches the line that represents the calculated ultimate tensile strength of stainless steel. When  $\varphi = 0$ , the corresponding values on the fitting curves in Figs 3 and 4 are the yield stress and ultimate tensile strength of aluminium, respectively. It can be seen from the experimental data that yield stress and ultimate tensile strength of bi-metals increase with increase in  $\varphi$ .

The relationship between bi-metals and plate elements is described as an exponential function, which is more precise. The relationship can be expressed as follows

$$\sigma = P - Qe^{C\varphi} \quad (14)$$



**Fig. 8** Macrographs of interface fracture (a) fracture side of stainless steel and (b) interface detachment

where  $\sigma$  is the yield stress or ultimate tensile strength, and  $P$ ,  $Q$ , and  $C$  are the correlation coefficients for the bi-metal.

Using the Monte-Carlo fitting method, the relationships of the yield stress  $\sigma_s$  and ultimate tensile strength  $\sigma_b$  to the relative thickness ratio of stainless steel are derived from the data points on the curves shown in Figs 3 and 4

$$\left. \begin{aligned} \sigma_s &= 569 - 330e^{-0.33\varphi} \\ \sigma_b &= 875 - 596e^{-0.29\varphi} \end{aligned} \right\} \quad (15)$$

#### 4.2 The relationships of elastic modulus $E$ , hardening coefficient $K$ , and hardening exponent $n$ to $\mathfrak{R}_{\text{stainless}}$

The relationships of  $E$ ,  $K$ , and  $n$  to  $\mathfrak{R}_{\text{stainless}}$  of the stainless steel–aluminium bi-metal are shown in Figs 5–7, respectively. It can be seen that the relationships of  $E$ ,  $K$ , and  $n$  to  $\mathfrak{R}_{\text{stainless}}$  basically take on a linear tendency. In addition,  $K$  increases fastest with  $\mathfrak{R}_{\text{stainless}}$ , followed by  $E$ , and  $n$  increases the slowest. The  $n$  value of the bi-metal lies between the  $n$  values of aluminium and stainless steel, and it shows an ascending tendency with the increase in  $\mathfrak{R}_{\text{stainless}}$ .

#### 4.3 Analysis of fracture and interface detachment

The standardized specimens under uniaxial tensile conditions show that fracture behaviours of the substrate, clad, and bi-metal all occur on the side of stainless steel. Obviously, the necking phenomenon appears but no fracture occurs on the side of the aluminium alloy since the lower strength material shows more intense plastic deformation. It can be seen from Fig. 8 that the detachment phenomenon takes place only on the bonding interface.

The reasons for the fracture phenomenon on the stainless steel side and the detachment on the bonding interface are as follows: First, the stainless steel has a considerably lower cross-section shrinkage rate than aluminium, and so aluminium shows larger localized plastic deformation than stainless steel. Second, the plastic strain ratio of stainless steel is larger than aluminium, leading to the frequent occurrence of deformation of the necking area on the side of stainless steel in the width direction. Third, stainless steel has a larger hardening exponent. Its localized deformation is hindered after the interface detachment, resulting in easy rupture of the stainless steel side. Fourth, when the effect of the stress in the width direction is considered, the stainless steel side is

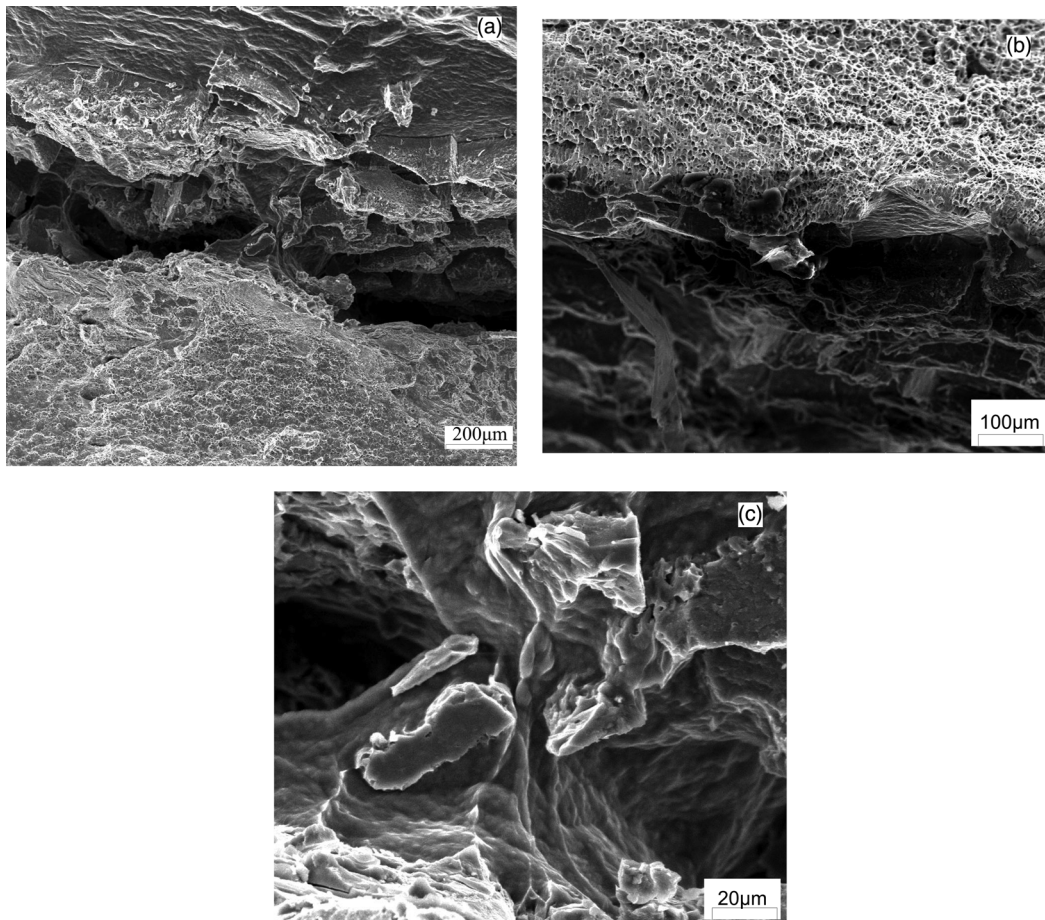


**Fig. 9** Micrographs of interface fracture: (a) unbound interface, (b) partly connected interface, and (c) local amplification of partly connected interface

under tensile strength while the aluminium side is under compression stress, which means that the stainless steel side is more vulnerable to rupture. Finally, according to Hill's local necking theory, a zero-strain line exists in the tensile-compression area of the bi-metal. In this study, the zero-strain line is located on the stainless steel side, indicating that this side is under great tensile strength. When the tensile strength reaches a certain large value, rupture will occur on this side.

Micrographs of interface fracture show that a large amount of detachment occurs on the interface region (Fig. 9(a)). Stainless steel and aluminium in localized areas fracture simultaneously; however, the interface still remains bonded (Fig. 9(b)). Although the fracture occurs on the interface, the fractured sections in the interface region are still partly interconnected (Fig. 9(c)).

## 5 CONCLUSIONS

1. The mechanical properties of the 1Cr18Ni9Ti–1A30 bi-metal are decided by its component materials. Yield stress and ultimate tensile strength show an exponent relation with the relative thickness ratio of stainless steel, while elastic modulus, hardening coefficient, and hardening exponent basically have a linear relationship with the absolute thickness ratio of stainless steel. All these relationships show a monotonic increasing tendency. Except for ultimate tensile strength, all the mechanical parameters calculated using the mixture rule theory are similar to the experimental data, which indicates that the mixture rule theory can be used to calculate most mechanical parameters; however, it is inappropriate for the calculation of ultimate tensile strength.
2. Stainless steel–aluminium tensile fracture behaviours mainly occur in the form of interface detachment on the stainless steel side of the bi-metal.

## ACKNOWLEDGEMENT

This work is supported by the National Eleventh Five-year Technology Support Project of China (No. 2006BAF04B14).

© Authors 2011

## REFERENCES

- 1 Liu, H. S., Yang, Y. Y., Yu, Z. Q., Sun, Z. Z., and Wang, Y. Z. The applications of a ductile fracture criterion to the prediction of the forming limit of sheet metals. *J. Mater. Process. Technol.*, 2009, **209**, 5443–5447.
- 2 He, M. and Hutchinson, J. Crack deflection at an interface between dissimilar elastic materials. *Int. J. Solids Struct.*, 1989, **25**, 1053–1069.
- 3 Kim, A., Besson, J., and Pineau, A. Global and local approaches to fracture normal to interfaces. *Int. J. Solids Struct.*, 1998, **36**, 1845–1864.
- 4 Liu, B. and Kimoto, H. Elastic–plastic analysis of a crack parallel to the interface. *Engng Fract. Mech.*, 1996, **53**, 607–623.
- 5 Wang, X. and Sudak, L. J. A piezoelectric screw dislocation interacting with an imperfect piezoelectric bimaterial interface. *Int. J. Solids Struct.*, 2007, **44**, 3344–3358.
- 6 Benveniste, Y. and Miloh, T. Imperfect soft and stiff interfaces in two dimensional elasticity. *Mech. Mater.*, 2001, **33**, 309–323.
- 7 Khelifa, M. and Oudjene, M. Numerical damage prediction in deep-drawing of sheet metals. *J. Mater. Process. Technol.*, 2008, **200**, 71–76.
- 8 Bäker, M. Simulation of crack propagation in mixed mode and at bimaterial interfaces using trial cracks. *Comput. Mater. Sci.*, 2009, **45**, 680–683.
- 9 Nowicke, F., Zavaliangos, A., and Rogers, H. C. The effect of roll and clad sheet geometry on the necking instability during rolling of clad sheet metals. *Int. J. Mech. Sci.*, 2006, **48**, 868–877.
- 10 Hungshiou, H. and Gowyi, T. Two analytical models of double-layer clad sheet compression forming based on the upper bound and the slab methods. *J. Mater. Process. Tech.*, 2003, **140**, 604–609.
- 11 Shatil, G., Saimoto, A., and Ren, X. J. Ductile-brittle fatigue and fracture behavior of aluminum/PMMA bimaterial 3PB specimens. *Engng Fract. Mech.*, 2008, **75**, 674–681.
- 12 Motarjemi, A. K., Kocak, M., and Ventske, V. Mechanical and fracture characterization of a bi-material steel plate. *Int. J. Press. Vessels Pip.*, 2002, **79**, 181–191.
- 13 Lei, Y. and Neale, B. The fracture behavior of a centre cracked tensile specimen. *Fract Engng Mater Struct.*, 1997, **20**, 201–216.
- 14 Sugimura, Y., Lim, P., Shih, C., and Suresh S. Fracture normal to a bi-material interface: effects of plasticity on crack tip shielding and amplification. *Acta Metall Mater.*, 1995, **43**, 1157–1169.

